Pathways of energy transfer in LHCII revealed by room-temperature 2D electronic spectroscopy

Kym L. Wells,[a] Petar H. Lambrev,[b] Zhengyang Zhang,[a] Gyözö Garab[b] and Howe-Siang Tan*[a]

We present here the first room-temperature 2D electronic spectroscopy study of energy transfer in the plant light-harvesting complex II, LHCII. Two-dimensional electronic spectroscopy has been used to study energy transfer dynamics in LHCII trimers from the chlorophyll b Q_y band to the chlorophyll a Q_y band. Observing cross-peak regions corresponding to couplings between different excitonic states reveals partially resolved fine structure at the exciton level that cannot be isolated by pump–probe or linear spectroscopy measurements alone. Global analysis of the data has been performed to identify the pathways and time constants of energy transfer. The measured waiting time (T_w) dependent 2D spectra are found to be composed of 2D decay-associated spectra with three timescales (0.3 ps, 2.3 ps and >20 ps). Direct and multistep cascading pathways from the high-energy chlorophyll b states to the lowest-energy chlorophyll a states have been resolved occurring on time scales of hundreds of femtoseconds to picoseconds.

Introduction

Light-harvesting antenna systems such as LHCII, the primary light-harvesting complex in plants, are essential for the photosynthetic process that eventually powers the biological world. The excitation energy transfer (EET) processes in naturally occurring light-harvesting systems are therefore of strong interest to scientists. Due to the ultrafast nature of these EET processes, femtosecond optical spectroscopy has proven to be a powerful tool to study these systems. Kwa et al.[1] used both one-colour and two-colour pump–probe spectroscopy to study the EET processes in LHCII trimers with ps time resolution. They observed energy transfer from chlorophyll b (Chl b) to chlorophyll a (Chl a) occurring in <1 ps, which they were unable to temporally resolve. They also observed a 2–6 ps process attributed to EET between the luminal and stromal layers of the complex. Bittner et al.[2] completed complementary studies with 250 fs time resolution which revealed a faster process of only ~150 fs which was attributed to EET from Chl b to Chl a. As in the work of Kwa et al., a 3–7 ps process was observed, which could be interpreted as EET from a different Chl b pool, or as redistribution of energy between Chl a excited states.

Separately collected transient absorption measurements of LHCII trimers by Visser et al.[3] and Connelly et al.[4] completed at

77 K each observed Chl b to Chl a EET processes with consistent time constants of 150–300 fs, 600 fs, and 4–9 ps. Similar measurements of LHCII monomers by Kleima et al.[5] found two comparable transfer times of ~200 fs and 3 ps. This work also involved global fitting of previously collected trimer[3] data with these measurements to determine that in both cases 50% of the transfer occurred on the ~200 fs timescale. It was concluded that the 600 fs process observed in the trimer is significantly slowed down in the monomer case to contribute to the observed ps process. The similarity between the monomer and the trimer results led the authors to conclude that Chl b to Chl a transfer is predominantly localised to individual monomers, which was later substantiated by theoretical studies that identified only one sizeable coupling between chlorophyll pigments on adjacent monomers in the trimer structure.[6] Recent polarized transient absorption measurements by Marin et al. at 77 K measured inter-monomer EET occurring within 3.3–5 ps across the entirety of the Q_y band.[7]

Significant efforts to model the spectral dynamics of LHCII have been undertaken.[8–11] Novoderezhkin et al.[6] and independently Linnanto et al.[9] and Renger et al.[12,13] using the 2.72 Å crystallographic LHCIIb structure[14] determined the energies of the 14 excitonic states that comprise the Q_y transitions of LHCII, encompassing both the Chl b and Chl a bands. They also modelled the heavily delocalised nature of these states using simultaneous quantitative fits of the linear absorption, linear dichroism, fluorescence spectra and transient absorption spectra. Other transient absorption experiments by van Grondelle and co-workers[15] on several recombinant isoforms of LHCII separated energy transfer dynamics from "red" and "blue"

[a] Division of Chemistry and Biological Chemistry, School of Physical and Mathematical Sciences, Nanyang Technological University, Singapore 637371, Singapore. E-mail: howesiang@ntu.edu.sg
[b] Institute of Plant Biology, Biological Research Centre, Hungarian Academy of Sciences, PO Box 521, H-6726, Szeged, Hungary

11640 | Phys. Chem. Chem. Phys., 2014, 16, 11640–11646

This journal is © the Owner Societies 2014

Chl b states to Chl a states with a sequential global fitting routine. They reported EET from high energy (blue) Chl b to Chl a occurring with a 600 fs and 4 ps time constant, and energy transfer from low energy Chl b (red) to Chl a occurring with time constants of 150 fs and 600 fs. However, it is not always possible in transient absorption measurements to unambiguously isolate contributions to peaks in the transient spectra originating from different initially excited states. Whilst 2D spectroscopy, by virtue of an extra frequency axis, is able to resolve the pump frequency as well as the emission frequency. Recently, 2D spectroscopy has been applied to probe LHCII. Schlau-Cohen et al.[16] identified cross peaks in the non-rephasing 2D spectra corresponding to Chl b to Chl a energy transfer. By observing these cross-peak amplitudes as a function of T_w, multistep dynamics occurring with a fastest, previously unrecorded <100 fs component were observed. These results suggest that multistep relaxation is occurring but no quantitative values were given.[16] Calhoun et al.[17] directly measured the energies of these excitonic states by observing the Fourier transform of the diagonal of the non-rephasing 2D spectra as a function of waiting time (T_w) at 77 K achieving excellent agreement with theory.

Presented here are 2D electronic spectroscopic studies of partially excitonically resolved energy transfer in LHCII at room temperature. At low temperatures the absorption spectra of LHCII are better resolved, but less representative of the physiological conditions under which light harvesting occurs. By performing the study presented in this paper at room temperature, we are moving to a regime which more closely mimics the *in vivo* conditions. Additionally, by tuning the spectrum of the first two interaction pulses to cover only the Chl b band, and using a white light continuum (WLC) to act as the third interaction pulse we observe the cross-peaks corresponding to Chl b to Chl a energy transfer without contribution from signals due to coherent processes which potentially complicate the interpretation of the collected 2D electronic spectra. In this study, we elucidate the energy transfer pathway from different spectral regions of the Chl b manifold to different spectral regions of the Chl a manifold.

In a similar approach to Schlau-Cohen's,[16] integrals corresponding to different excitonic couplings on a purely absorptive 2D spectra are collected at a range of T_w values, to observe real-time energy transfer. To date, few room temperature multidimensional spectroscopy studies of light harvesting complexes have been completed.[18–20] To develop a true understanding of the efficiency of light harvesting systems *in vivo*, studies must start to be tailored to more closely match physiological conditions.

Experimental

The experimental setup and theory behind the phase cycling schemes necessary for these pump–probe geometry 2D electronic spectroscopy measurements have been well described[21,22] and demonstrated[23] previously, as has the use of a white light continuum (WLC) probe and necessary chirp considerations associated with this.[24–26] Only a brief description of the experimental set-up is provided here. By utilizing a pump–probe geometry set-up with phase cycling the absorptive 2D spectra are recovered directly. In a traditional boxcar arrangement both the 2D rephasing and 2D non-rephasing signals need to be collected, phased and summed to yield the purely absorptive 2D spectra. The phasing needs to be performed with great care to separate the real and imaginary parts of the 2D purely absorptive spectrum without causing distortion to the observed lineshape.[20,27,28] In pump–probe geometry 2DES, wherein the first two interaction pulses are collinear allowing the simultaneous measurement of the rephasing and non-rephasing signals, the phasing step is unnecessary. Thus, there is no ambiguity in the peak shape arising from inadequate phasing.

LHCII trimers were isolated and purified from spinach thylakoid membranes, solubilized with α-dodecyl maltoside (α-DM) by sucrose-gradient ultracentrifugation as described in the work of Caffarri et al.[29] Before measurements, the LHCII suspension was diluted with nitrogen-flushed 0.06% α-DM and 10 mM HEPES buffer solution to provide an optical density of 0.27 (at the Chl a Q_y maximum) in a 1 mm sapphire-windowed sample cell. All measurements were collected at room temperature (298 K). A commercially available regenerative amplifier laser system (Legend Elite, Coherent) provided pulses centred at 800 nm (0.8 W, 1 KHz, 40 fs) which pumped a home-built optical parametric amplifier (OPA). The near-infrared output of the OPA was subsequently frequency doubled to be resonant with the Q_y transition of the Chl b band of LHCII at 15 385 cm^{-1} (650 nm) with a FWHM of $\sim$350 cm^{-1} ($\sim$14 nm), which was sufficiently broad to excite the entirety of the Chl b exciton manifold. This beam was passed through a commercially available acousto-optic programmable dispersive filter[30] (Dazzler, Fastlite) to generate the first two excitation pulses, with variable time delay and relative phase. All measurements presented here were referenced to a carrier frequency of 14 277 cm^{-1} (700 nm), to place the signal into the partially rotating frame, taken with a 1 × 2 phase cycling scheme[22,23] and attenuated to 70 nJ sum energy for the two pulses. The pulse shaper further compressed the pulses to 55 fs FWHM. The combined third interaction pulse and local oscillator was a white light continuum generated by focussing a small amount of the fundamental frequency beam (800 nm) through a 2 mm sapphire window, and passing over a delay stage to enable control of the population time (T_w) after the first two excitation pulses. The shaped laser output and the WLC were overlapped on the sample cell, with the WLC subsequently dispersed with a spectrometer (Acton SP2300, Princeton Instruments) onto a CCD detector (PIXIS 100B, Princeton Instruments). The linear absorption spectra were taken before and after measurement scans to confirm that sample degradation had not occurred.

The first two interaction pulses were scanned over a total time range of 180 fs in 3 fs steps, whilst the T_w value remained constant. Due to the presence of a coherent artefact at short T_w, only 2D electronic spectra (2DES) at T_w larger than 150 fs were analysed. 2DES were collected at T_w values extending to 12.5 ps. In each collected 2DES presented here, the two frequency axes can be viewed as 'pump' (ω_τ) and 'probe' axes (ω_t) where the

This journal is © the Owner Societies 2014

Phys. Chem. Chem. Phys., 2014, **16**, 11640–11646 | **11641**

frequency-resolved excitation of the 'pump' is correlated with the frequency-resolved absorption of the 'probe' after a waiting time T_w. Since for these measurements a WLC is used to provide the third interaction field and local oscillator, the true T_w value for each ω_t in each 2DES is different according to the chirp of the WLC. For the data analysis presented here the T_w is corrected according to the relative observation time of the coherent artefact at each ω_t.

Results

2D spectra and time evolution

Fig. 1 shows the linear absorption spectrum of the Q_y bands of LHCII at room temperature, with the Chl a band and Chl b band centred at $\sim 14\,800$ cm^{-1} and $\sim 15\,375$ cm^{-1} respectively. The spectrum of the pump pulse (the first two interaction pulses) used in these measurements is overlaid. The stick plots indicate the positions of the excitonic states comprising these bands, according to the model of Novoderezhkin *et al.*[6]

Fig. 2 shows typically collected purely absorptive 2DES at a selection of T_w values. All 2DES are plotted on the same intensity scale. The diagonal of the 2D spectrum for $T_w = 0.3$ ps is overlaid as a white dashed line. A qualitative description of the trends and features of the 2D spectra is provided here, followed by a quantitative study detailed below. All 2DES show two features. Firstly, a diagonal feature ($\omega_\tau = \omega_t$) corresponds to the Chl b excitonic diagonal signals. Since the first two excitation pulses do not spectrally overlap with Chl a excitonic states, neither diagonal signals nor signals due to quantum coherences[31] are observed in the Chl a spectral region. At $T_w > 5$ ps the Chl b diagonal signal vanishes, indicating that energy transfer out of the Chl b states is fully completed within this time.

The second feature is an off-diagonal peak ($\omega_\tau = 15\,400$ cm^{-1}, $\omega_t = 14\,800$ cm^{-1}), rising in amplitude over $T_w < 10$ ps, which corresponds to energy transfer from the initially excited Chl b excitonic states to Chl a excitonic states. The decay of the cross-peak at $T_w > 10$ ps is indicative of relaxation to the ground state. The broad peak is composed of a number of overlapping cross-peaks corresponding to energy transfer between different
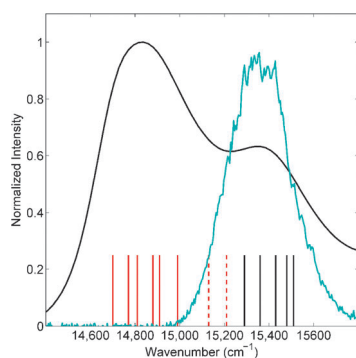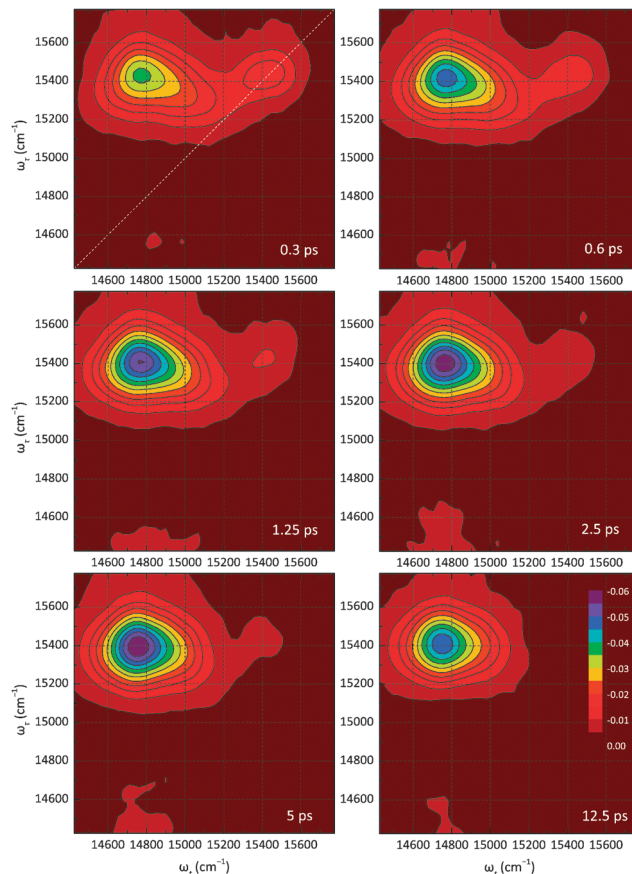

Fig. 2 Purely absorptive 2DES recorded at waiting times $T_w = 0.3$, 0.6, 1.25, 2.5, 5 and 12.5 ps. The same colour–coding scale is used for all spectra, with red colour representing the positive signal and blue colour representing the negative signal. The axes correspond to the "pump" frequency ω_τ and the "probe" frequency ω_t.

Fig. 1 Linear absorption spectrum of LHCII trimers (black) and the spectrum of the first two interaction pulses used in the 2DES measurements (blue). Stick plots – Chl a based excitonic states (red) and predominantly Chl b based excitonic states (black).[6,17]

excitonic states. The principal relationship guiding the interpretation of the 2D spectra is that a cross-peak appearing at the intersection of a "pump" frequency ω_τ and a "probe" frequency ω_t, which we will denote as $\omega_\tau \rightarrow \omega_t$, is a result of energy transfer from an excitonic state with resonance frequency ω_τ to a state with resonance frequency ω_t. The intensity of the cross peak over time follows the population, or concentration, of the acceptor state resulting from the respective EET process.

Although individual exciton states cannot be resolved because of the large spectral overlap, the shape of the cross-peak reveals substantial information regarding the pathways and dynamics of EET. As can be seen from Fig. 2, at sub-ps waiting times the main cross-peak is broader and asymmetric due to the population of different excitonic states of various energies. At longer waiting times, as excitation energy is concentrated on the lowest-energy Chl a excitonic states, the peak becomes narrower, symmetric and its midpoint shifts to lower frequencies. In particular one can easily notice that at $T_w = 0.3$ ps there is a relatively high intensity at the intersection $15\,300 \rightarrow 15\,000$ cm^{-1}. It can be inferred that an energy level corresponding to $15\,000$ cm^{-1} is populated from an exciton state at *ca.* $15\,300$ cm^{-1} over a time scale of 0.3 ps. At the same time, the cross-peak amplitude at

$15\,500 \rightarrow 15\,000$ cm^{-1} is significantly lower, indicating that these two frequencies are not strongly coupled. Energy from the $15\,500$ cm^{-1} level flows to exciton(s) positioned at $14\,800$ cm^{-1} instead. The feature at the intersection $15\,300 \rightarrow 15\,000$ cm^{-1} disappears gradually with increasing T_w. Another conclusion that can be drawn directly from the shape of the 2D spectra is that the $15\,000$ cm^{-1} state is long-lived – visible even at $T_w = 12.5$ ps.

The intensity of the 2D spectra at several frequency intersections is plotted as a function of waiting time in Fig. 3. The first panel (Fig. 3a) traces the intensity along the diagonal ($\omega_\tau = \omega_t$), showing the decay of Chl b excited states. It is immediately apparent that higher-energy states decay faster than lower-energy states. The next three panels group time traces representing EET from different Chl b frequencies to a single Chl a frequency. Rather than decay, these traces show the rise in Chl a excited-state population. In Fig. 3b, high-energy Chl a states ($15\,000$ cm^{-1}) are rapidly populated and then slowly decay over several ps. In Fig. 3d, slow, picoseconds rise kinetics is observed for the lowest-energy states ($14\,600$ cm^{-1}). Comparing the time traces plotted in the same panel, *i.e.* at one ω_t, some notable differences are revealed. The $15\,300 \rightarrow 15\,000$ cm^{-1} trace rises to a maximum in 1 ps, affirming the strong coupling between these two frequencies, and then slowly decays following the depopulation of the intermediate state at $15\,000$ cm^{-1}. In contrast, the $15\,500 \rightarrow 15\,000$ cm^{-1} curve has lower amplitude, slower rise and no significant decay. In comparison, the $15\,500 \rightarrow 14\,800$ cm^{-1} trace rises quickly to a maximum and then decays, whereas the $15\,300 \rightarrow 14\,800$ cm^{-1} trace shows a biphasic rise over the chosen time range. Finally, the traces representing EET to the lowest-energy Chl a do not significantly depend on the pump frequency. These slowly populated states are the final acceptors of excitation energy as indicated by the slow continuous rise at $T_w > 5$ ps (in contrast, the signal at higher frequencies decays on this time scale).
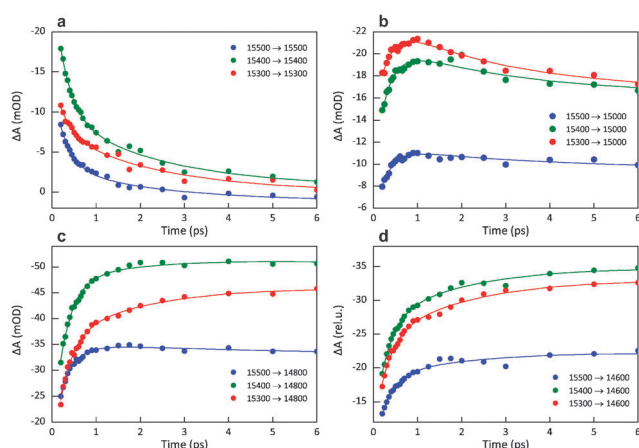
We must reiterate that due to spectral overlap the time traces for different $\omega_\tau \rightarrow \omega_t$ obviously sum up the EET among multiple excitonic states. While it is tempting to relate the cross-peak frequencies to calculated excitonic levels, *e.g.* those calculated by Calhoun *et al.*,[17] there are complications such as inhomogeneous broadening, spectral diffusion[32] and Stokes' shifts of the excited-state emission contributing to the non-linear spectra.

Global analysis of the 2D spectral evolution

To obtain a quantitative measure of the lifetimes of the system and qualitative information about the processes occurring on each lifetime, we present the results of a global analysis of the 2D spectra to recover 2D decay-associated spectra (2D DAS). The global analysis procedure (written in MATLAB) relies on the assumption that the diagonal peaks as well as the cross-peaks in the 2D spectra follow the kinetics of the excited state population in the system, which can be described as a sum of exponential components.[33,34] The time-dependent 2D absorptive signal at any given frequency pair ω_τ, ω_t is then described by the equation:

$$\Delta A(\omega_\tau, \omega_t, t) = \sum_{i=1}^{n} D_i(\omega_\tau, \omega_t) \cdot e^{-t/\Gamma_i}$$

where $t = T_w$, Γ_i are the lifetimes of the system, n is the total number of lifetime components, and $D_i(\omega_\tau,\omega_t)$ are 2D DAS for the respective lifetimes. Note that the lifetimes are independent of frequency, *i.e.* the kinetics for every frequency pair is described with the same set of lifetimes. The absorptive 2D spectra taken at a range of population times T_w were simultaneously fitted according to such a model, whereby the lifetimes were determined by a global iterative non-linear least squares minimization algorithm. The method of variable projection was applied[33] to separate the nonlinear parameters (lifetimes) from the linear parameters (pre-exponential amplitudes $D_i(\omega_\tau,\omega_t)$ comprising the 2D DAS). The latter were calculated by linear regression at every iteration of the minimization. Prior to the analysis, the 2D data were corrected for dispersion (chirp) of the probe light, determined from a conventional pump–probe measurement performed with the same experimental setup. In this present study, the instrument response function (IRF) is not taken into consideration. However in future studies the IRF may need to be included in the analysis, especially for time-scales comparable to the laser pulse widths.

A minimum of three lifetimes was necessary to achieve a good fit of the 2D spectra – 0.30 ps, 2.3 ps, and $\gg$10 ps. The number of time points and the signal-to-noise level limit the number of lifetimes that can be resolved. Since the fit was performed only in the time region of 0.2–8 ps, the longest lifetime is not accurately determined. Time trace fits produced by the analysis are displayed in Fig. 3 as solid lines.

The 2D DAS resulting from the global analysis are shown in Fig. 4. In general the DAS associated with a given lifetime is a linear combination of the spectra of all absorbing species (exciton states) whose concentration changes with this lifetime.[33] In the 2D DAS, negative peaks (in blue) indicate decay,

Fig. 3 Time traces of the absorptive 2D signal at selected frequency intersections, indicated in the plots as $\omega_\tau \rightarrow \omega_t$. The top-left panel represents diagonal signals ($\omega_\tau = \omega_t$) and the rest – cross-peak signals. Each point in the time traces is the integrated 2D signal from an area of *ca.* 50 cm^{-1} × 50 cm^{-1}. Symbols represent the experimentally measured data points and solid lines show the best fit using a global three-exponential analysis with lifetimes of 0.3, 2.3 and 175 ps across all ω_τ/ω_τ.

This journal is © the Owner Societies 2014

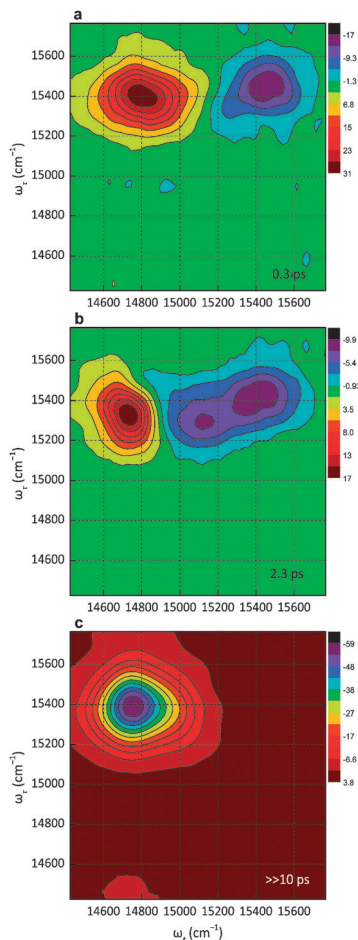*Phys. Chem. Chem. Phys.*, 2014, **16**, 11640–11646 | **11643**

Fig. 4 2D decay-associated spectra resulting from a global fit of the 2D spectra with three exponential terms. The respective lifetimes are indicated in the plots (lower-right corner). Blue colours represent negative pre-exponential amplitudes, *i.e.* decay of the bleaching signal, and red colours represent positive amplitudes, *i.e.* rise of the bleaching signal. The first two 2D DAS show rise of the cross-peak, centered at $\omega_t \sim 14\,800$ cm^{-1}, and the final DAS shows decay of the cross-peak.

Fig. 5 Horizontal slices of the 2D DAS for τ = 0.3 ps and τ = 2.3 ps at selected pump frequencies ω_τ, showing EET originating from excitonic states with the respective transition resonance frequency ω_τ.

whereas positive peaks (in red) indicate rise of the bleaching signal. On a 2D DAS, the occurrence of a negative peak and a positive peak along the same ω_τ frequency strongly suggests EET from frequency ω_t of the negative peak to the frequency ω_t of the positive peak. Thus, the 2D DAS corresponding to the first two lifetimes, 0.3 and 2.3 ps (Fig. 4a and b, respectively), indicates EET, and the 2D DAS with the longest lifetime depicted in Fig. 4c indicates decay to the ground state.

The first 2D DAS (Fig. 4a) reveals that on a time scale of 300 fs Chl *b* excited states with energies around 15 400 cm^{-1} transfer energy to Chl *a* excited states between 14 600 and 15 000 cm^{-1}. It is rather clear from this DAS that there is ultrafast, femtosecond-scale EET to a broad range of Chl *a* frequencies, including the lowest ones (<14 700 cm^{-1}). The positive peak can also be seen to be non-circular and aligned in an anti-diagonal fashion. This indicates that the lower energy acceptor excitons are correlated with the higher energy donor excitons. To further aid in understanding the 2D DAS, slices of the 0.3 ps lifetime 2D DAS at selected ω_τ frequencies are plotted
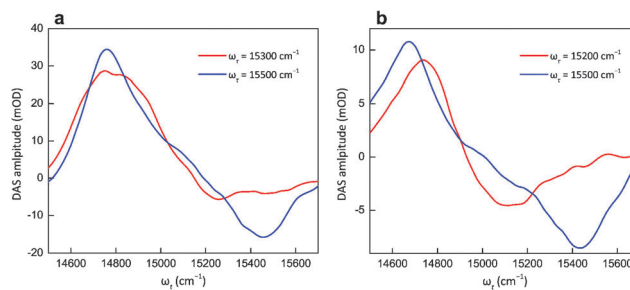
in Fig. 5a. The positive part of the curves can be regarded as the spectrum of Chl *a* states that are populated by EET from the selected ω_τ frequency. Note that the negative peak position, representing the decay of the donor states, approximately matches the selected pump frequency. On a sub-ps time scale, the sliced DAS show EET from a frequency of 15 300 cm^{-1} to the high-energy intermediate (14 900–15 000 cm^{-1}) and from 15 500 cm^{-1} to the main Chl *a* band (14 800 cm^{-1}). This is consistent with the 15 300 → 15 000 cm^{-1} cross-peak found in the 2D spectrum at T_w = 0.3 ps (Fig. 2).

The second 2D DAS (Fig. 4b) represents slow EET processes, occurring on a time scale of 2.3 ps. From the shape of the 2D DAS, three main conclusions can be drawn. First, EET from the higher-energy Chl *b* states to Chl *a* occurs on this slower time scale as well. Hence, there is a long-lived population of Chl *b* states not connected by fast EET to either Chl *b* or Chl *a*. Comparing the amplitude of the negative Chl *b* peak in the two DAS, it can be found out that 33% of the Chl *b* states decay with the slower lifetime. Second, a distinguishing feature of the 2.3 ps 2D DAS is the negative cross-peak 15 300 → 15 100 cm^{-1}. The cross-peak indicates the presence of a long-lived intermediate Chl *a* state at ~15 100 cm^{-1}, populated by rapid EET from a Chl *b* state at 15 300 cm^{-1} and then decaying *via* slow (picoseconds) EET to the lower-energy Chl *a*. In Fig. 5b, horizontal slices at ω_τ = 15 200 cm^{-1} and 15 450 cm^{-1} of the 2D DAS of Fig. 4b are taken. The plots reveal EET from 15 500 cm^{-1} to the lowest-energy Chl *a* (14 600 cm^{-1}) as well as downstream energy flow from the intermediate level of 15 000–15 200 cm^{-1}. These DAS slices corroborate the finding that high-energy Chl *b* states (15 450 cm^{-1}) are coupled to low-energy Chl *a* (14 670 cm^{-1}), with EET between them occurring on two time scales – hundreds of femtoseconds and a few picoseconds. Lastly, the slower 2.3 ps 2D DAS reveals equilibration in the lower energy Chl *a* manifold, where mid-energy Chl *a* states (14 800–14 900 cm^{-1}) decay to the lowest-energy states, causing the comparatively narrow and skewed Chl *a* cross-peak.

The third and final 2D DAS, associated with the longest lifetime ($\gg$10 ps), represents the decay of Chl *a* excited states.

The DAS do not explicitly reveal whether the EET is a direct or a multistep process involving intermediate excitonic states. In fact from the DAS slices it seems that the 2.3 ps EET from 15 450 cm^{-1} to 14 670 cm^{-1} is a multistep process *via* states

at $\sim 14\,900$ cm^{-1}. For a definitive answer to the question of multistep EET, 2DES data of substantially higher dynamic range and time resolution are needed (in order to resolve more lifetimes) or, alternatively, a 3D experimental setup with an additional frequency axis.

Discussion

The pump–probe geometry 2DES results presented here partially resolve the EET pathways between Chl *b* and Chl *a* excitonic states in LHCII at room temperature. To our knowledge, this is the most detailed experimentally obtained EET kinetics scheme so far. Whilst the identified cross-peak regions studied here are not fully resolved, differences between couplings of different initially excited excitonic states are clearly evident, which pump–probe measurements alone cannot observe.

In a short summary, our qualitative and quantitative global data analysis suggests: (1) fast (≤ 300 fs) EET from high Chl *b* levels (15 400–15 500 cm^{-1}) to middle Chl *a* levels (14 800 cm^{-1}); (2) fast EET from lower Chl *b* levels (15 200–15 300 cm^{-1}) to the intermediate level (15 000–15 100 cm^{-1}); (3) on a much slower, picoseconds time scale, another population (33%) of Chl *b* states decays *via* EET to Chl *a*; (4) slow relaxation from the high-energy Chl *a* intermediate to the lowest Chl *a* levels; (5) equilibration in the low-energy Chl *a* manifold also occurs on this slower time scale.

The Chl *b* manifold can be divided into two groups, with one located near the stromal side and the other near the luminal side. The two groups are physically separated from each other, which can be the reason why we can observe two distinct lifetimes of EET from Chl *b*. According to the theoretical models and numerical simulations based on transient absorption, and other steady state spectroscopies, developed in the work of van Grondelle and Novoderezhkin,[8,11] there is no fast energy relaxation from the Chl *b* manifold to the lowest-energy Chl *a* states. However, our 2DES experiments unambiguously demonstrate such EET. The model of van Grondelle and Novoderezhkin predicts fast energy relaxation from the luminal Chl *b* group (Chls 606 and 607) to the high-energy Chl *a* 604. This fast EET is probably the origin of the cross peak at 15 300 → 15 100 cm^{-1} in Fig. 2. Also in agreement with the model, and with previous low-temperature 2DES experiments,[16] the high-energy Chl *a* state is weakly coupled to the low-energy Chls and is thus a bottleneck state that decays on a time scale of several ps. Our experiments clearly distinguish the bottleneck state with a resonant frequency of about 15 000 cm^{-1} and further show the fast coupling of this state to the low-energy Chl *b* (15 300 cm^{-1}).

A parallel can also be drawn between our work and ultrafast transient absorption experiments done on CP29, another member of the LHCII family, which has a highly similar pigment arrangement, except that a few Chl *b* pigments found in the major LHCII are replaced by Chl *a* in the CP29 structure.[35] Croce *et al.*[36] have observed three lifetimes of EET from Chl *b* (15 400 cm^{-1}) to Chl *a* in CP29 – 150 fs, 1.2 ps and 5–6 ps. The present analysis of the 2D cannot resolve all lifetimes in the system but the general finding of a fast-decaying (300 fs) and a slow-decaying (2 ps) population of Chl *b* is in agreement with these earlier experiments. Probably the longest lifetime in CP29 involves high-energy Chl *a* intermediates as well. Finally, our experimental data point to a slower, pico-seconds equilibration kinetics within the Chl *a* domain, in line with the structure-based theoretical predictions of Renger *et al.*[13]

Not all excitonic states can be unambiguously resolved in our experiments and therefore it is not possible to determine all states and pathways based on these experimental data alone. Furthermore, we have not included the contributions from direct excitation of the first vibronic replica of the Chl *a* Q_y bands by the first two interaction pulses. However since absorptivity of these bands is much smaller than the main Chl *b* Q_y bands, their contributions are minor, although this warrants further studies and simulations.

Whilst polarization controlled measurements have shown great promise in isolating specific spectral features in 2DES,[37–39] it is unlikely that these methods will provide unambiguous assignment of the multistep mechanisms involved here. It is thus suggested that higher dimensional spectroscopy measurements, such as those already demonstrated on solvated Chl *a*,[40,41] are needed to further clarify the intermediate excitonic states involved in these step-wise energy transfer processes, as higher dimensional spectroscopy will reveal higher order couplings. These multi-step pathways are most likely due to spatial overlap of excitonic states of mixed Chl *a* and Chl *b* composition with both the high-energy Chl *b* excitonic states and the low-energy Chl *a* excitonic states. To truly understand the efficiency of naturally occurring light-harvesting complexes, and indeed energy transfer processes in larger pigment–protein complexes, a much refined understanding of the energy transfer mechanisms at physiological temperatures is required.

Acknowledgements

Notes and references

1 S. L. S. Kwa, H. van Amerongen, S. Lin, J. P. Dekker, R. van Grondelle and W. S. Struve, *Biochim. Biophys. Acta*, 1992, **1102**, 202–212.

2 T. Bittner, K. D. Irrgang, G. Renger and M. R. Wasielewski, *J. Phys. Chem.*, 1994, **98**, 11821–11826.

3 H. M. Visser, F. J. Kleima, I. H. M. van Stokkum, R. van Grondelle and H. van Amerongen, *Chem. Phys.*, 1996, **210**, 297–312.

This journal is © the Owner Societies 2014

Phys. Chem. Chem. Phys., 2014, **16**, 11640–11646 | **11645**

4 J. P. Connelly, M. G. Muller, M. Hucke, G. Gatzen, C. W. Mullineaux, A. V. Ruban, P. Horton and A. R. Holzwarth, *J. Phys. Chem. B*, 1997, **101**, 1902–1909.

5 F. J. Kleima, C. C. Gradinaru, F. Calkoen, I. H. M. van Stokkum, R. van Grondelle and H. van Amerongen, *Biochemistry*, 1997, **36**, 15262–15268.

6 V. I. Novoderezhkin, M. A. Palacios, H. van Amerongen and R. van Grondelle, *J. Phys. Chem. B*, 2005, **109**, 10493–10504.

7 A. Marin, I. N. M. van Stokkum, V. I. Novoderezhkin and R. van Grondelle, *J. Photochem. Photobiol., A*, 2012, **234**, 91–99.

8 R. van Grondelle and V. I. Novoderezhkin, *Phys. Chem. Chem. Phys.*, 2006, **8**, 793–807.

9 J. Linnanto, J. Martiskainen, V. Lehtovuori, J. Ihalainen, R. Kananavicius, R. Barbato and J. Korppi-Tommola, *Photosynth. Res.*, 2006, **87**, 267–279.

10 V. I. Novoderezhkin and R. van Grondelle, *Phys. Chem. Chem. Phys.*, 2010, **12**, 7352–7365.

11 V. Novoderezhkin, A. Marin and R. van Grondelle, *Phys. Chem. Chem. Phys.*, 2011, **13**, 17093–17103.

12 F. Müh, M. Madjet and T. Renger, *J. Phys. Chem. B*, 2010, **114**, 13517–13535.

13 T. Renger, M. E. Madjet, A. Knorr and F. Müh, *J. Plant Physiol.*, 2011, **168**, 1497–1509.

14 Z. F. Liu, H. C. Yan, K. B. Wang, T. Y. Kuang, J. P. Zhang, L. L. Gui, X. M. An and W. R. Chang, *Nature*, 2004, **428**, 287–292.

15 M. A. Palacios, J. Standfuss, M. Vengris, B. F. van Oort, I. H. M. van Stokkum, W. Kuhlbrandt, H. van Amerongen and R. van Grondelle, *Photosynth. Res.*, 2006, **88**, 269–285.

16 G. S. Schlau-Cohen, T. R. Calhoun, N. S. Ginsberg, E. L. Read, M. Ballottari, R. Bassi, R. van Grondelle and G. R. Fleming, *J. Phys. Chem. B*, 2009, **113**, 15352–15363.

17 T. R. Calhoun, N. S. Ginsberg, G. S. Schlau-Cohen, Y. C. Cheng, M. Ballottari, R. Bassi and G. R. Fleming, *J. Phys. Chem. B*, 2009, **113**, 16291–16295.

18 G. Panitchayangkoon, D. Hayes, K. A. Fransted, J. R. Caram, E. Harel, J. Z. Wen, R. E. Blankenship and G. S. Engel, *Proc. Natl. Acad. Sci. U. S. A.*, 2010, **107**, 12766–12770.

19 E. Collini, C. Y. Wong, K. E. Wilk, P. M. G. Curmi, P. Brumer and G. D. Scholes, *Nature*, 2010, **463**, 644–U669.

20 J. M. Anna, E. E. Ostroumov, K. Maghlaoui, J. Barber and G. D. Scholes, *J. Phys. Chem. Lett.*, 2012, **3**, 3677–3684.

21 H.-S. Tan, *J. Chem. Phys.*, 2008, **129**, 124501.

22 S. Yan and H.-S. Tan, *Chem. Phys.*, 2009, **360**, 110–115.

23 Z. Zhang, K. L. Wells, E. W. J. Hyland and H.-S. Tan, *Chem. Phys. Lett.*, 2012, **550**, 156–161.

24 P. E. Tekavec, J. A. Myers, K. L. M. Lewis and J. P. Ogilvie, *Opt. Lett.*, 2009, **34**, 1390–1392.

25 P. F. Tekavec, J. A. Myers, K. L. M. Lewis, F. D. Fuller and J. P. Ogilvie, *Opt. Express*, 2010, **18**, 11015–11024.

26 P. A. Tekavec, K. L. M. Lewis, F. D. Fuller, J. A. Myers and J. P. Ogilvie, *IEEE J. Sel. Top. Quantum Electron.*, 2012, **18**, 210–217.

27 J. D. Hybl, A. W. Albrecht, S. M. G. Faeder and D. M. Jonas, *Chem. Phys. Lett.*, 1998, **297**, 307–313.

28 D. B. Turner, K. E. Wilk, P. M. G. Curmi and G. D. Scholes, *J. Phys. Chem. Lett.*, 2011, **2**, 1904–1911.

29 S. Caffarri, R. Croce, J. Breton and R. Bassi, *J. Biol. Chem.*, 2001, **276**, 35924–35933.

30 A. Monmayrant, A. Arbouet, B. Girard, B. Chatel, A. Barman, B. J. Whitaker and D. Kaplan, *Appl. Phys. B: Lasers Opt.*, 2005, **81**, 177–180.

31 A. Ishizaki, T. R. Calhoun, G. S. Schlau-Cohen and G. R. Fleming, *Phys. Chem. Chem. Phys.*, 2010, **12**, 7319–7337.

32 K. L. Wells, Z. Y. Zhang, J. R. Rouxel and H. S. Tan, *J. Phys. Chem. B*, 2013, **117**, 2294–2299.

33 I. H. M. van Stokkum, D. S. Larsen and R. van Grondelle, *Biochim. Biophys. Acta*, 2004, **1657**, 82–104.

34 A. R. Holzwarth, in *Biophysical Techniques in Photosynthesis*, ed. J. Amesz and A. J. Hoff, Kluwer Academic Publishers, Dordrecht, 1996, pp. 75–92.

35 X. W. Pan, M. Li, T. Wan, L. F. Wang, C. J. Jia, Z. Q. Hou, X. L. Zhao, J. P. Zhang and W. R. Chang, *Nat. Struct. Mol. Biol.*, 2011, **18**, 309–315.

36 R. Croce, M. G. Müller, R. Bassi and A. R. Holzwarth, *Biophys. J.*, 2003, **84**, 2508–2516.

37 G. S. Schlau-Cohen, T. R. Calhoun, N. S. Ginsberg, M. Ballottari, R. Bassi and G. R. Fleming, *Proc. Natl. Acad. Sci. U. S. A.*, 2010, **107**, 13276–13281.

38 N. S. Ginsberg, J. A. Davis, M. Ballottari, Y. C. Cheng, R. Bassi and G. R. Fleming, *Proc. Natl. Acad. Sci. U. S. A.*, 2011, **108**, 3848–3853.

39 G. S. Schlau-Cohen, E. De Re, R. J. Cogdell and G. R. Fleming, *J. Phys. Chem. Lett.*, 2012, **3**, 2487–2492.

40 Z. Zhang, K. L. Wells and H.-S. Tan, *Opt. Lett.*, 2012, **37**, 5058–5060.

41 Z. Zhang, K. L. Wells, M. T. Seidel and H.-S. Tan, *J. Phys. Chem. B*, 2013, **117**, 15369–15385.

11646 | *Phys. Chem. Chem. Phys.*, 2014, **16**, 11640–11646

This journal is © the Owner Societies 2014